Geophys. J. Int. (2000) **142,** 000–000

On the minimum of vertical seismic noise near 3 mHz

W. Zürn[1] and E. Wielandt[2]

[1] *Black Forest Observatory (Schiltach), Universities Karlsruhe/Stuttgart, Heubach 206, D-77709 Wolfach, Germany*
e-mail: walter.zuern@gpi.uni-karlsruhe.de
[2] *Institute of Geophysics, University of Stuttgart, Azenbergstrasse 16 70174 Stuttgart, Germany*
e-mail: wielandt@geophysik.uni-stuttgart.de

January 30, 2006

SUMMARY
Acceleration power spectral densities of vertical seismic noise at the best seismic stations show a minimum near 3 mHz. We suggest that this minimum is caused by a cancellation near this frequency of Newtonian attraction vs. free air and inertial effects exerted by atmospheric phenomena on the sensor mass. Simplistic models of atmospheric phenomena are used to quantify this effect and examples are shown for special atmospheric events.
Key words: vertical seismic noise, barometric pressure, long periods

1 "GEDANKENEXPERIMENTS"

Consider a parcel of air above a vertical accelerometer (seismometer or gravimeter) changing its density sinusoidally around the mean value. At the moment of maximum density Newtonian attraction on the sensor mass will be upward. At the same moment barometric pressure will have a maximum and so will the downward deflection of the crust at the site. This in turn will increase downward gravity (the free air effect). Upward ground acceleration at this moment is maximum and in turn, the inertial (d'Alembert force) effect on the sensor mass will be maximum downward. Thus the latter two forces are in opposite direction to the Newtonian effect. Since the inertial force depends strongly on the frequency of the density oscillation but the other two forces do not, these three effects will cancel each other at some frequency.

In contrast, consider a vertical plane through the site of a horizontal seismometer sensing accelerations perpendicular to this plane. Now let the half-atmosphere to the right change its density sinusoidally around the value of the half to the left. The Newtonian attraction of the sensor mass will be maximum to the right, when the density has its maximum. Simultaneously, downward deflection at some distance to the right will be maximum and the sensor will experience maximum tilt towards the right, thus the Earth's gravity produces a force on the sensor into this direction. At this same moment the horizontal displacement at the site will be maximum to the right and the d'Alembert force will point into the same direction. So for horizontal components all three forces add, while for vertical components Newtonian attraction is opposed by the free air and inertial effects in a frequency dependent manner. We suggest that these physical principles and the fact that the atmosphere is the major source of long period noise cause the different behaviour of vertical and horizontal sensors in terms of observed long period noise at the best stations. Noise of instrumental origin or caused by insufficient shielding from the immediate environment is explicitly excluded in the above statement.

In the following we will discuss these ideas more explicitely and quantitavely using simplistic models of atmospheric phenomena in the long period seismic band.

2 INTRODUCTION

Peterson (1993) has defined the so-called New Low Noise Model (NLNM) for vertical seismic noise. This model represents the lower envelope of a large set of power spectral densities (PSD) obtained from many quiet vertical seismograms from many stations of the Global Digital Seismic Network (GSN). Quiet in this work means: free of clear earthquake signals and clear instrumental or man-made disturbances, but tides were not removed from the data. This model is widely used for reference. New work has been done along similar lines by Berger et al. (2004) and current noise estimates from the global network in comparison to the NLNM can be found in the World Wide Web at *http://www.seismology.harvard.edu/...*. The NLNM is shown in Fig. 1 for vertical acceleration. This model shows one broad minimium between about 2.5 and 25 mHz with a small hump near about 6-10 mHz. This paper deals with the minimum to the left of this hump.

Horizontal noise is usually higher by factors of 5 to 10 especially at long periods and strongly dependent on the method of installation. A number of noise estimates for comparison can again be found in the work by Berger et al. (2004) and on the website mentioned above. Even the best horizontal noise spectra do not show these two minima but roll off monotonically with increasing frequency in the spectral range where the NLNM has this minimum. However, another minimum in horizontal seismic noise also exists at about 20 mHz (Agnew 1986). Probably below this frequency the noise from atmospheric loading is

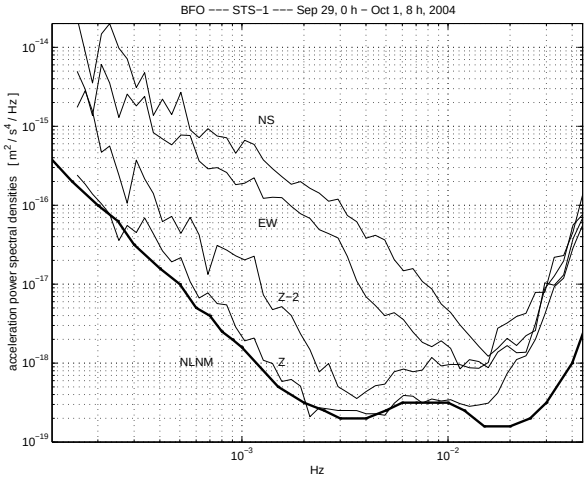

Fig. 1. Acceleration power spectral densities for 56 hour long records of the STS-1 seismometers at station BFO. Solid lines labeled Z, EW and NS are from the corresponding components for the very quiet 56 h interval starting September 29, 0:00:00 GMT, 2004. Note the large difference between the vertical and horizontal components. The thick solid line represents the NLNM of Petersen (1993). Z follows the NLNM closely up to about 12 mHz. The difference between EW and NS is due to an amplification of pressure-induced noise on the latter component due to a cavity-effect (King et al. 1976). The curve labeled Z-2 is for the vertical component during the barometrically noisy 56 h interval starting 0:00:00 GMT on October 29, 2004 for comparison.

dominant and above it the oceanic noise rises sharply to the microseismic peaks. However, horizontal noise is not the subject of this paper.

Fig. 1 also shows examples of acceleration noise power spectral densities from the three STS-1 seismometers (Z, NS, EW) (Wielandt and Streckeisen 1982) at the mine observatory BFO ($48.33^o N, 8.33^o E$) described by Richter et al. (1995), which is known for its low noise levels especially at long periods (Beauduin et al. 1996, Freybourger et al. 1997, Banka and Crossley 1999, Van Camp 1999, Berger et al. 2004). The vertical component shows the broad minimum while the horizontals do not.

In the following we will discuss a possible physical explananation for the existence of the minimum near 3 mHz in the NLNM for vertical accelerations by extending the model from the first "Gedankenexperiment" above to more detailed but still very simplistic models of interactions between the local atmosphere, the solid earth and the seismic sensors.

Agnew and Berger (1978) in an earlier paper on vertical seismic noise suggest that the high noise in gravimeter records from coastal and island sites could be caused by oceanic edge waves. Such sites are not reaching the low noise levels of the NLNM. Since we discuss here the lowest achievable noise levels, only the best sensors at the best stations are considered. Instrumental effects and high noise sites are not the subject of this paper.

It is important at very long periods to realize that a vertical accelerometer senses different physical forces from the same geophysical phenomenon: the inertial effect dominating at high frequencies, the free air effect due to vertical motion, change in gravitation due to mass redistribution in the displacement field (Gilbert 1980) and direct Newtonian gravitation from the source (for example the moon and sun in the case of Earth tides). Additional effects exist, for example Coriolis and centrifugal forces due to the rotation of the Earth (e. g. Zürn et al. 2000), but these are mostly negligible compared to the four above. In Table 1 we list for vertical accelerometers the contribution of these four physical effects to the signals from different geophysical phenomena.

3 NOISE MECHANISMS BELOW 0.007 HZ

3.1 Newtonian attraction below 2 mHz

At frequencies below about 0.5 cph (0.14 mHz) it is well established by work on tidal gravity, that after removing the Earth tides from a record one sees a residual signal which is clearly correlated with the local barometric pressure (e. g. Warburton and Goodkind 1977). Therefore in modern tidal analysis of gravity data the local barometric pressure signal is included in the model for the tides and a simultaneous least squares solution is obtained. The resulting regression factors are of the order of 3.0 to 4.3 nm/s^2/hPa and are explained by the variable Newtonian attraction of the sensor mass by the changing density distribution in the whole atmosphere but with the air above the sensor weighted very strongly. Additionally the air masses load the crust and cause a variable displacement field which in turn produces smaller and opposite gravity signals due to the associated mass redistributions and free air effects.

Two simple models of the atmosphere can be used to demonstrate that the regression factors found experimentally make physical sense. First take an extremely simple atmosphere above an infinite half-space with density ρ_o constant to a height H_o and zero above (the Bouguer plate model, BPM). The gravity effect of this atmosphere is $2 \cdot \pi \cdot G \cdot H_o \cdot \rho_o$, the pressure p at the bottom of it is simply $g_o \cdot \rho \cdot H_o$, where G is the gravitational constant and g_o is the gravitational acceleration. Identical equations apply to variations of density $\Delta\rho$, gravity Δg and pressure Δp. The theoretical coefficient between the local gravity effect and pressure becomes

$$\frac{\Delta g}{\Delta p} = -\frac{2 \cdot \pi \cdot G}{g_o} = -4.27\ nm/s^2/hPa. \qquad (1)$$

Since the free air and mass distribution effects have opposite sign to the Newtonian effect, the observed regression coefficient has to be smaller in magnitude than this estimate.

A slightly more realistic atmospheric model is an isothermal one, where density varies exponentially with height z: $\rho = \rho_o \cdot exp(-z/H)$ where H is now the scale height of the atmosphere. The theoretical coefficient in this case is

$$\frac{\Delta g}{\Delta p} = \frac{-2\pi G \Delta\rho_o \int_o^\infty exp(-z/H) \cdot dz}{\Delta\rho_o g_o \int_o^\infty exp(-z/H) \cdot dz} = -\frac{2\pi G}{g_o} \qquad (2)$$

as before. It is obvious from eq. (2) that any density distribution $\rho(z)$ in the integrals will lead to the same factor as long as it is laterally homogeneous and flat (a stack of Bouguer plates). Of course, these models are extremely simplistic and several modifications have been suggested to improve the efficiency of the corrections of gravity records especially at very long periods. Due to the curvature of the Earth at periods longer than the daily tides a smaller admittance is expected (because the distant atmosphere will be below the horizon) and also experimentally

Table 1. Relative contributions (in %) by relevant forces of phenomena sensed by vertical accelerometers. Negative contributions are 180^o out of phase with positive ones. The amplitudes can only be compared within one line. Note the increasing importance of the inertial effect with rising frequency. For the tides the contributions to the gravimetric factor are listed. The data for the free modes were taken from Dahlen and Tromp (1998, table 10.1). ${}_1S_1$ is the Slichter mode. The fifth example corresponds to the crossover between free air and inertial effect for a simple harmonic vertical motion like on a shake table or calibration platform. AGW stands for the atmospheric acoustic-gravity wave as modeled by Neumann and Zürn (1999).

Signal	Frequency	Inertial	Free air	Mass redistr.	Gravitation
M_2-tide	22.4 μHz	0.34	52.00	-39.00	86.66
M_3-tide	33.0 μHz	0.26	17.71	-11.19	92.32
${}_1S_1$	0.0513 mHz	3.20	96.00	0.80	0.0
${}_oS_2$	0.309 mHz	81.86	66.53	-48.39	0.0
Crossover	0.28 mHz	50.00	50.00	0.0	0.0
AGW	1 mHz	-30.67	-2.67	0.0	133.33
${}_oS_{10}$	1.726 mHz	98.20	2.60	-0.80	0.0
Rayleigh-Wave	0.05 Hz	100.00	0.0	0.0	0.0
P-wave	1.0 Hz	100.00	0.0	0.0	0.0

found (e. g. Boy et al. 1998). Also barometric pressure variations at exactly one cycle per day and integer multiples of that frequency (e. g. S_n waves) belong to phenomena in the atmosphere distinctly different from the broadband variations outside of these frequencies and therefore at these frequencies different admittances are again expected and observed (Warburton and Goodkind 1977).

Zürn and Widmer (1995) realized that the simple regression with local barometric pressure and admittances near 3.5 nm/s^2/hPa is effective up to 1 to 2 mHz and thus allows to improve the signal-to-noise ratio (SNR) in vertical records of the gravest free oscillations of the Earth. They showed that modes hidden in the noise can on occasion be clearly seen after the correction. Virtanen (1996) and Van Camp (1999) demonstrated this effect also using records from superconducting gravimeters. Beauduin et al. (1996) also succeeded in reducing the noise PSDs for vertical component records from STS-1 seismometers at the GEOSCOPE stations SSB (France) and TAM (Algeria) using the locally recorded barometric pressure. Fig. 2 shows an example for the efficiency of this correction for the record of the N-Sumatra-Andaman Islands quake of December 26, 2004 from the superconducting gravimeter at Bad Homburg, Germany.

Zürn and Widmer (1995) also showed that for excellent gravimeters the noise levels after the correction can fall below the NLNM for frequencies below 1 mHz. Modeling shows that most of this effect is caused by Newtonian attraction of the sensor mass with only little contribution from loading (e. g. Table 1, AGW). It was also found that for frequencies higher than 1 - 2 mHz the noise level increases after application of the correction with a simple factor. This is not a problem really since low-pass filtering of the barometric pressure record before correcting the data will avoid this problem completely. This simplistic method worked also very well in the modeling of the gravity effect of an atmospheric gravity wave since the frequencies involved were well below 1 mHz (Neumann and Zürn 1999).

Müller and Zürn (1983) calculated analytically the vertical gravitational force exerted by an atmosphere consisting of

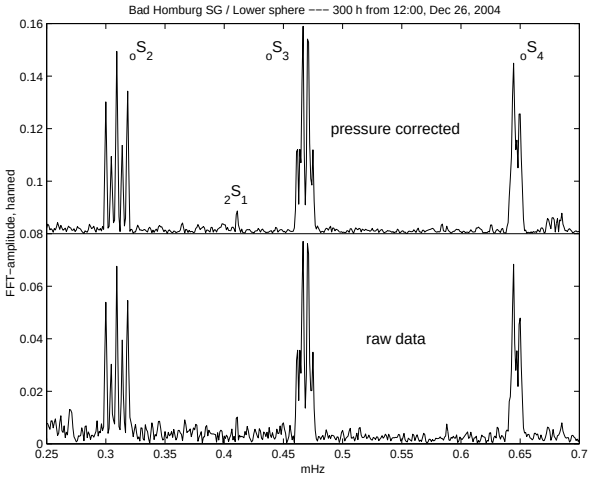

Fig. 2. Fourier spectra after hanning 300 hour time series starting at 12:00 GMT, December 26, 2004 from the superconducting gravimeter GWR-CD030 (lower sphere) showing the lowest order spheroidal modes excited by the N-Sumatra-Andaman Islands earthquake. The bottom panel is from the raw data, the top panel from the same data after correction with local atmospheric pressure using a factor of 3.5 $nm/s^2/hPa$. Note the very clear enhancement of the signal-to-noise ratio, in particular for ${}_2S_1$ at 0.41 *mHz*.

two air masses with different ground level densities separated by a vertical plane (a cold front) above a rigid halfspace with the densities falling off exponentially with height as in the second model above (isothermal BPM). As the front moves from $-\infty$ to $+\infty$ the total gravity change is also given by eq. (1). The authors compared observed gravity signals with theoretical ones computed using the observed pressure increase and temperature drop to estimate the density change. Since the observations were obtained with a bandpass-filtered gravity record the speed of the front had to be specified as well and a value of 10 m/s was used. This value resulted from estimating the average speed of cold fronts from weather maps (24 hours apart).

Müller (1981) reports 14.4 m/s for a cold front observed in the vicinity of BFO with a tripartite microbarograph network. In the numerical computations the front was shaped according to specifications in meteorology textbooks (parabolic). Fair agreement between theoretical and observed amplitudes and polarities was obtained for several cold front passages. This result corroborates the explanation of the noise in this frequency band by Newtonian attraction of the sensor mass by the atmosphere.

Widmer-Schnidrig (2003) and Zürn and Widmer-Schnidrig (2003) report that the simplistic correction works well with the best gravimeters. At times when barometric fluctuations are small, power spectral densities below the NLNM are obtained, when the fluctuations are large, at least the NLNM is reached. This is not the case for STS-1/Z seismometers. Only when the fluctuations are large can the SNR be improved by the correction. For STS-2/Z the noise below 1 mHz is dominated by instrumental effects. For other broadband seismometers we have no experience for this frequency range. The NLNM obviously describes the lower limit obtainable by STS-1/Z seismometers. The lowest noise levels below 0.8 to 1 mHz are now achieved by the latest generation of superconducting gravimeters (SG) when the barometric correction is applied to the data. The fact that the lowest noise levels of SGs reached for atmospherically quiet and noisy days differ basically proves that the simple correction does not take the full pressure effect out of the data. Indeed, Meurers (2000) detected gravity variations in this band with the SG in Vienna in connection with rain showers without a corresponding change in barometric pressure. He tried to explain the effect by vertical transport of water in the atmosphere above the site. Simon (2003) identified such effects in extremely long period gravity records and used radiosonde data to model them.

In any case, below about 1 mHz it is clear from the efficiency of the noise reduction in gravimeters with the help of local barometric pressure and from modeling that the vertical noise is dominated by the deterministic effects of the atmosphere and to the largest part by Newtonian attraction. This point was missed by Tanimoto (1999), who tried to explain the long period seismic noise statistically by atmospheric turbulence (see Tanimoto and Um 1999 for a correction).

3.2 Frequency band 2 to 7 mHz: The hum

Around 1998 Japanese seismologists detected that by stacking spectra of quake-free records of vertical component seismograms from gravimeters and STS-1/Z seismometers one can see the incessantly excited fundamental spheroidal oscillations (hum) of the Earth between 2 and 7 mHz (e. g. Nawa et al. 1998, Suda et al. 1998, Tanimoto et al. 1998, Nishida et al. 2000, Ekström 2001). At first the favored source of these vibrations was the atmosphere (Tanimoto and Um 1999, Fukao et al. 2002). Seasonal changes in the amplitudes of these modes and the typically enhanced amplitude of ${}_oS_{37}$ (close to the fundamental vertical free mode of the atmosphere) with respect to its neighbours lead to this conclusion. This atmospheric mode was first detected in seismograms during the violent eruption of Mount Pinatubo (Philippines) on June 15, 1991 (Kanamori and Mori 1992, Widmer and Zürn 1992, see also Lognonné et al. 1998). Recent work by Rhie and Romanowicz (2004) and Tanimoto (2005) attempted to identify the energy source for the excitation of the hum as infragravity waves in the oceans. Of course, those would be driven by the atmosphere and also result in seasonal variations.

The power in these modes obviously represents the lower limit of vertical seismic noise between 2 and 7 mHz at a level of less than the NLNM minimum at roughly $3.2 \cdot 10^{-19}$ m^2/s^3. We make this statement because the background modes can not be identified in the spectra of single 12 - or 24 - hr windows. The noise one sees in such a window in this frequency band is probably the result of three contributions: instrumental noise, the background modes and inertial effects from local barometric loading as we try to show below. The latter contribution would be non-stationary, of course (Widmer-Schnidrig 2003, Zürn and Widmer-Schnidrig (2003). If global barometric fluctuations are really the cause of the background modes then there is basically no reason for the excitation to stop at 2 and 7 mHz, respectively; the modes outside of and adjacent to this band should be excited to similar amplitudes. Above about 7 mHz the effects of lateral heterogeneities on the locations of the spectral peaks of fundamental spheroidal mode multiplets becomes so severe that the hum cannot be detected by stacking many spectra (e. g. Dahlen and Tromp, 1998). However, both Ekström (2001) and Nishida et al. (2002) show that the vertical noise at frequencies from 7 up to 20 mHz consists of fundamental Rayleigh wave energy (the surface wave equivalent of fundamental spheroidal modes). At frequencies below 2 mHz the acceleration noise rises steeply due to the Newtonian attraction by the (local) atmosphere as discussed above which in turn is due to the rising power of the barometric pressure fluctuations (about proportional to period squared). Incessantly excited modes will be buried more deeply in the local noise than above 2 mHz. Neither atmosphere nor oceans are able to excite ${}_oS_o$ (or any other radial mode) since the total weight of these masses is constant.

4 ATMOSPHERIC NOISE MODELS INCLUDING THE INERTIAL EFFECT

4.1 Bouguer Plate Model

Table 1 demonstrates that for any phenomenon deforming the Earth the inertial force on the sensor due to ground acceleration dominates at the higher frequencies. The simple BPM above was only taking the Newtonian attraction into account. We now improve BPM slightly by taking either the homogeneous or isothermal atmosphere and let it exert pressure on the surface of an elastic layer with Lamé parameters λ and μ and thickness D above a rigid halfspace, and by adding the free air and inertial effects (from now on IBPM). When the air density in the atmosphere and (consequently) the atmospheric pressure on the elastic layer vary harmonically with angular frequency ω (we assume implicitly that the density at every altitude and the surface pressure are in phase) the depression of the surface will be

$$\Delta z = \frac{D}{\lambda + 2\mu} \cdot \Delta p \tag{3}$$

and consequently the admittance between pressure variation Δp and vertical acceleration Δg becomes

$$\frac{\Delta g}{\Delta p} = -\frac{2 \cdot \pi \cdot G}{g_o} + \frac{D}{\lambda + 2\mu} \cdot (\omega^2 + \left|\frac{\delta g}{\delta z}\right|) \tag{4}$$

where $|\delta g/\delta z|$ is the vertical gravity gradient at the surface and z the vertical coordinate. The additive terms on the right hand side are Newtonian gravitation, inertial and free air effects, respectively. The mass redistribution effect is neglected here (see below).

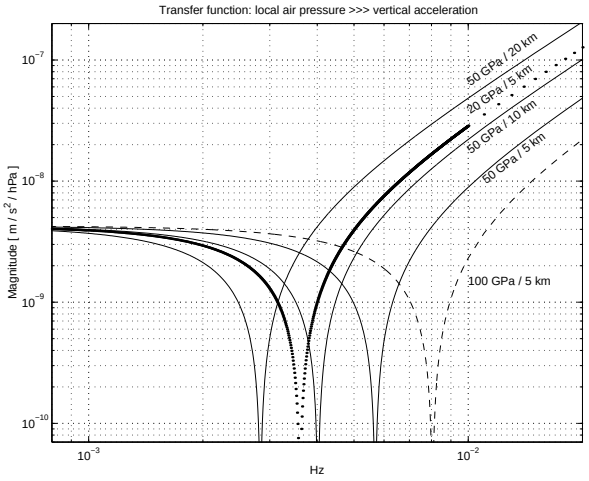

Fig. 3. Magnitude of transfer functions from barometric pressure to vertical acceleration for the elastic Bouguer Plate Model (IBPM) from eq. (3). Lam´e Parameters $\mu = \lambda$ and elastic layer thickness D are given at each curve.

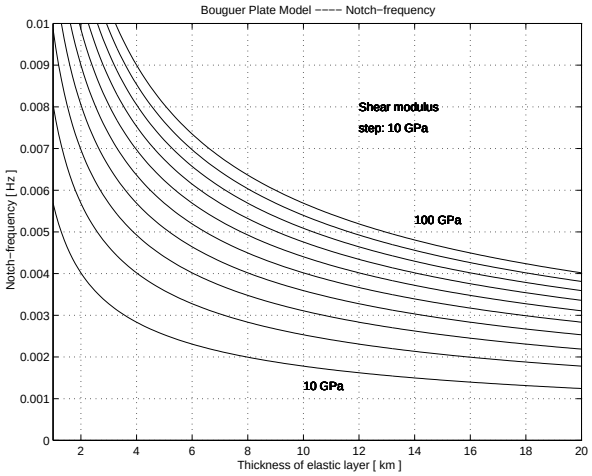

Fig. 4. Frequency of zero (eq. (4)) of the transfer function for IBPM from pressure to vertical acceleration as function of depth D of elastic layer with shear modulus $\mu = \lambda$ as parameter of the different curves.

The second two contributions have opposite polarity to the first one. Therefore a frequency ω_o exists for each model of the halfspace below the atmosphere where the effects exactly cancel each other and the total admittance changes polarity.

$$\omega_o^2 = \frac{2 \cdot \pi \cdot G}{g_o} \cdot \frac{\lambda + 2\mu}{D} - \left| \frac{\delta g}{\delta z} \right| \tag{5}$$

This equation has of course no real solution for ω_o^2 if the first term is numerically smaller than the second. This condition translates obviously into a condition for $(\lambda + 2\mu)$ being smaller than a certain numerical value which turns out to be two orders of magnitude smaller than the average rigidy of the crust (incidentally this value is very close to the lithostatic pressure at the base of the elastic layer).

Fig. 3 shows the frequency dependent admittance (eq. (4)) for several models of the crust. The polarity change moves to higher frequencies with increasing rigidity of the elastic layer and with decreasing thickness D. For this model f_0 does not depend on any property of the atmosphere, only on the parameters describing the elastic layer.

Fig. 4 shows curves of the notch-frequency $f_0 = \omega_0/(2\pi)$ versus D with μ as a parameter. Fig. 5 depicts for two days the vertical acceleration noise predicted from the local pressure variations. The first time interval is barometrically very quiet, the second one very noisy. The predicted noise may be compared with the actually observed noise shown in Fig. 1.

This model does not take into account that pressure fluctuations are associated with air masses of finite extent and that the size of these air masses decreases with increasing frequency. A typical spatial scale to time scale ratio for atmospheric phenomena is 10 m/s (Fortak, 1971), but clearly this is a strong simplification, which is mostly valid for convective phenomena. For sound and gravity waves the ratio of wavelength to period is given by the phase velocity. Frontal systems have different extent in lateral than in propagation direction.

4.2 Modified Warburton-Goodkind Model

Warburton and Goodkind (1977) also developed a model (from here on WG77) for the atmospheric effects on gravimeters. Un-

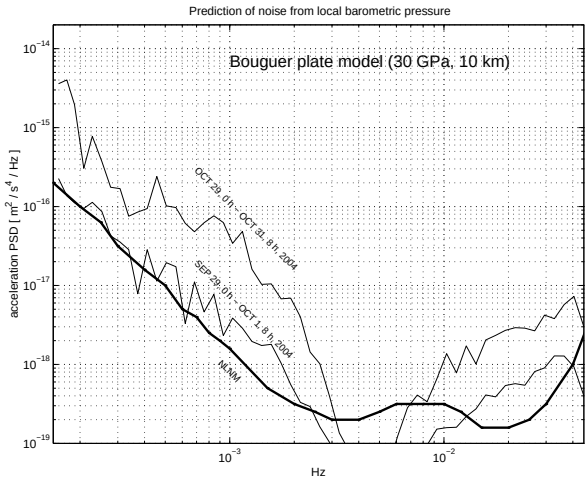

Fig. 5. Prediction of vertical acceleration PSD using IBPM and local barometric pressure for two 56 hour time series as labeled. The PSDs may be directly compared to the observed PSDs in Fig. 1. NLNM shown by thick solid line.

fortunately the authors do not specify explicitly several facts so for example we can only guess that the free air effect and the mass redistribution effects are included, but certainly the inertial effect is not. Their model consists of a circular cylinder with radius R imbedded into a standard atmosphere. The relative difference of the density inside and outside the cylinder is the same at all altitudes. The parameter describing this model is the pressure difference Δp below the cylinder. The effects are only considered at the surface in the center of the cylinder. Their Earth model is spherical but specified only by a single combination of Lamé parameters. They determine the effects of gravity decrease by direct Newtonian attraction and the gravity increase due to the deformation of the Earth. They find that the vertical displacement $\Delta z = constant \cdot R \cdot \Delta p$ at the center of the cylinder. Clearly, for harmonic pressure variations the inertial effect is in phase with the free air effect and so again at a certain frequency there will be a complete compensation of all the contributions. The effect of Newtonian attraction of a cylinder

with constant density, radius R and height H at the surface in the symmetry axis is (e. g. Dobrin, 1960)

$$\frac{\Delta g_N}{\Delta p} = -\frac{2 \cdot \pi \cdot G}{g_o} \cdot (1 + b_1 \cdot \frac{R}{H} - \sqrt{b_1^2 \cdot \frac{R^2}{H^2} + 1}) \qquad (6)$$

with $b_1 = 1$. Unfortunately Warburton and Goodkind (1977) present results only in their Fig. 3. In order to be able to approximate their result (for the standard atmosphere density profile) we introduced the adjustment factor b_1 into the equation above. From their Fig. 3 we determine b_1 to approx. 0.936. From the same figure we find the admittance for free air and mass redistribution effects to be a linear function of R and describe this by

$$\frac{\Delta g_{F,R}}{\Delta p} = \kappa_1 \cdot b_2 \cdot R \qquad (7)$$

with $\kappa_1 = 1.58 \cdot 10^{-17}\ m^2/s^2/Pa$ determined from this Fig. 3. In order to allow for other crustal properties we introduced the factor b_2 (equal to 1 for their crustal elasticity). Assuming the mass redistribution contribution to be small compared to the free air effect (see below) and a standard vertical gradient of gravity we can approximately determine the size of the vertical displacement and in turn the corresponding inertial effect for this model

$$\frac{\Delta g_I}{\Delta p} = \kappa_2 \cdot b_2 \cdot R \cdot \omega^2 \qquad (8)$$

with $\kappa_2 = 5.28 \cdot 10^{-12}\ Pa^{-1}$.

Since there must be a relation between the spatial and temporal scales of atmospheric phenomena we introduced an additional proportionality factor ψ between R and $1/\omega$ with $R = \psi/\omega$ (for waves $\psi = 2 \cdot \pi \cdot c$ with the phase velocity c and R the wavelength). The total effect for this extended model (WG77) valid on the symmetry axis at the bottom of the cylinder becomes

$$\begin{aligned} \frac{\Delta g}{\Delta p} &= -\frac{2\pi G}{g_o} \cdot (1 - \sqrt{b_1^2 \frac{\psi^2}{\omega^2 H^2} + 1} \cdots \\ &\quad + b_1 \cdot \frac{\psi}{\omega H}) + b_2 \psi (\frac{\kappa_1}{\omega} + \kappa_2 \omega) \end{aligned} \qquad (9)$$

The factors b_1 and b_2 are of the order of 1 and ψ is describing the cell size as a function of frequency. If the l.h.s of eq. (9) is set to zero, one has a fourth order polynomial equation for ω_o, i. e. the frequency at which gravity signals from this model vanish. Numerically one finds two real solutions, one at higher frequencies near 3.5 mHz, where free air and inertial effects cancel the Newtonian attraction as for the IBPM. The other solution is found at much lower frequencies, where the inertial effect is negligible and the other two effects cancel each other. The latter is due to the second term in eq. (9) which unrealistically grows to infinity as ω gets very small. However, the model is also very unrealistic in the sense, that atmospheric cells with different sizes (frequencies) cannot be active at the same time centered above the point of observation. The next model is much more realistic than the two models described so far.

4.3 Acoustic-Gravity Wave Model

An important atmospheric phenomenon in the frequency band under discussion are acoustic-gravity waves (AGW, e. g. Gossard and Hooke 1975, Nappo 2002, Nishida et al. 2005). Neumann (1997), Neumann and Zürn (1999) and Zürn (2002) calculated the signals produced by a plane sinusoidal density wave

$$\rho(x, y, z, t) = \hat{\rho} \cdot exp(-\frac{z}{H\gamma}) \cdot exp(j(k_h \cdot x - \omega \cdot t), \qquad (10)$$

where $j = \sqrt{-1}$, and the resulting pressure distribution with

$$\hat{p}(x, y, z, t) = c^2 \cdot \hat{\rho} \qquad (11)$$

travelling in x-direction along the surface of an elastic halfspace (λ and μ as above) with horizontal phase velocity c_h and horizontal wave number $k_h = \omega/c_h$. c is the sound velocity. The scale height H is now slightly differently defined $H \cdot \gamma/c^2 = 1/g_o$ as compared to the IBPM (with the adiabatic coefficient $\gamma = c_p/c_v$, the ratio of specific heats at constant pressure and volume, respectively). In contrast to the IBPM the elastic halfspace in not limited. This model is a good description of a Lamb wave (e. g. Gossard and Hooke 1975), but only for the loading effects a good model for a general AGW, since those travel at an angle to the Earth's surface and the density distribution depends not only on z. The horizontal phase velocities of such waves range between 10 m/s and 330 m/s. The vertical accelerometer is located at x_a, $y_a = 0$ and $z_a = 0$. The r. h. s. of the equations (13), (15) and (16) have to be multiplied by the factor

$$exp(j(k_h \cdot x_a - \omega \cdot t)) \qquad (12)$$

The result for the Newtonian attraction of the sensor mass by the air is (Neumann 1997)

$$\Delta g_z^N(x_a, z_a = 0) = 2 \cdot \pi \cdot G \cdot \frac{\hat{p}}{c^2} \cdot \frac{H \cdot \gamma}{1 + k_h H \gamma} \qquad (13)$$

Upward acceleration is positive here and for extremely long wavelength $k_h = 0, \omega = 0$ and $c_h = \infty$ the r. h. s. gives the result of eqs. (1) and (2) again. The ratio of the vertical attractions for the BPM and the AGW is

$$\frac{\Delta g_z^N}{\Delta g_z^{BPM}} = \frac{1}{1 + \frac{c^2}{g_o} \cdot \frac{\omega}{c_h}} \qquad (14)$$

which equals one when ω = 0.

The equations of motion for the elastic solid are treated quasistatically, i. e. the inertial terms are dropped because the phase velocities of the atmospheric waves are at most equal to the sound velocity of 330 m/s. The displacement field was calculated following Sorrells (1971). From its components the following contributions are derived. The free air effect due to the vertical displacement of the sensor in the undisturbed gravity field of the Earth is

$$\Delta g_z^F(x_a, z_a) = -\left|\frac{\delta g}{\delta z}\right| \frac{1}{2\mu} \left[\frac{\lambda + 2\mu}{\lambda + \mu}\right] \frac{1}{k_h} \hat{p} \qquad (15)$$

where $|\delta g/\delta z|$ is the local vertical gravity gradient. The inertial effect associated with this motion is

$$\Delta g_z^I(x_a, z_a) = -\frac{1}{2\mu} \cdot \left[\frac{\lambda + 2\mu}{\lambda + \mu}\right] \cdot \frac{\omega^2}{k_h} \cdot \hat{p} \qquad (16)$$

Sorrells (1971) only derived the inertial effect because he did not consider the long periods discussed here. Incidentally, in the derivation of this equation in his paper printing errors are abundant, but the final formula corresponding to the eq. (16) above is correctly printed. Again the Newtonian attraction effect has the opposite sign to the inertial and free air effects. Fig. 6 shows the transfer function magnitude as a function of frequency with

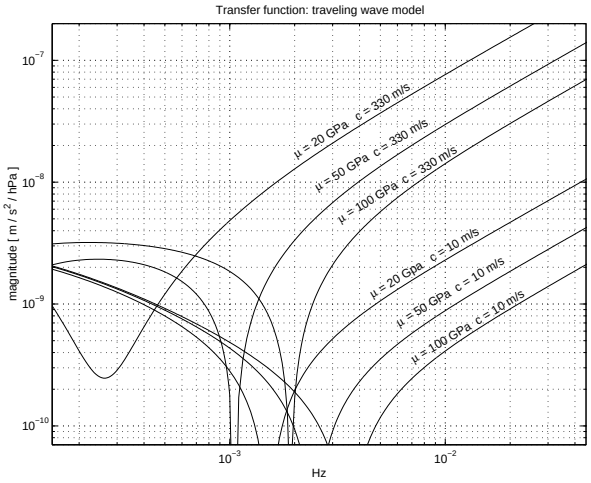

Fig. 6. Magnitudes of transfer-function from local barometric pressure to vertical acceleration for the AGW-model vs. frequency. Extreme values for the horizontal phase velocity of the waves and three different values for $\mu = \lambda$ were used as parameters. Note the rather shallow notch for the leftmost curve.

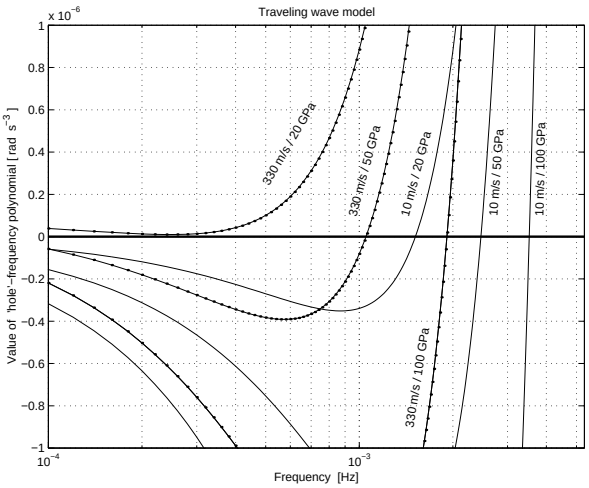

Fig. 7. Third order polynomials for the notch-frequency f_0 as function of frequency of the waves. Curves are labeled with horizontal phase velocity c_h and Lam´e parameters $\mu = \lambda$ of the halfspace. The leftmost curve (330 m/s and 20 GPa) has no zero-crossing in this frequency range.

shear modulus $\mu = \lambda$ and horizontal phase velocity c_h as parameters for several models of this kind. Conspicuously higher values of c_h enhance the rise to higher frequencies due to the inertial effect. This is caused by the larger horizontal wavelength $\lambda_h = 2\pi c_h/\omega$ which results in larger amplitude of the vertical displacement and consequently free-air and inertial effects get larger.

Again there are angular frequencies ω_0 at which the effects all cancel each other. Let $\lambda = \mu$ for simplicity, then these frequencies must satisfy the following polynomial equation

$$\omega_0^3 + \frac{c_h g_0}{c^2}\omega_0^2 + \omega_0 \left(\left| \frac{\delta g}{\delta z} \right| - \frac{8\pi G\mu}{3c^2} \right) + \left| \frac{\delta g}{\delta z} \right| \frac{c_h g_0}{c^2} = 0 \quad (17)$$

This polynomial in ω_0 is plottet in Fig. 7 versus $f_0 = \omega_0/(2\pi)$ for two extreme horizontal phase velocities and three values of the shear modulus μ. The notch-frequencies for each model are the values where the polynomial vanishes. The only term which may become negative and could cancel the others is the linear one. Assuming the standard gravity gradient at earth's surface the expression in the parentheses is indeed negative for $\mu \geq 0.585GPa$, a value almost two orders of magnitude below values for the Earth's crust.

However, because of the other positive terms, this threshold occurs at higher values of μ as can be seen for the curve with parameters μ = 20 GPa and c_h = 330 m/s in the diagram. The zeros in Fig. 7 are spread through the range of frequencies containing the minimum of the NLNM.

4.4 Mass Redistribution

In the models above (except WG77) we neglected the secondary gravity effect due to mass redistribution in the earth as a consequence of the deformation. Rabbel and Zschau (1985) estimated numerically the gravity changes and deformations on a Gutenberg-Bullen Earth model due to circular pressure cells with a pressure anomaly of the form $\Delta p(r) = \Delta p_{max} \cdot exp(-r^2/r_o^2)$. They evaluated two models with r_o equal to 160 and 1000 km. They found that the direct attraction effect was again well correlated with the local pressure with regression factors of $\approx$ 4 nm/s^2/hPa, that the mass redistribution effect correlated well with the vertical displacement u_z with a regression factor of 440 $nm/s^2/m$ and that the total gravity perturbation still correlated with local pressure with factors between 3 and 4 $nm/s^2/hPa$. The mass redistribution effect for these two models is about 15 % of the free air effect for a standard vertical gravity gradient. At this level a complication arises from the fact that the mass redistribution will somehow depend on the horizontal wavenumber and thus on frequency and therefore the notch would certainly be shifted slightly in frequency. Considering the speculative and approximative nature of the IBPM, WG77, and AGW-models to explain the atmospheric contribution to the noise it appears that our neglecting the mass redistribution effect is justified.

5 EXAMPLES

In the frequency band between 2 and 25 mHz STS-1 seismometers are at present the vertical sensors with the highest sensitivity (e. g. Widmer-Schnidrig, 2003). We therefore tried to experimentally estimate the transfer function from local barometric pressure to vertical ground acceleration using data from this sensor at the quiet site BFO. 11-day time series (September 20, 0:00:00.0 UT until September 30, 23:59:55.0, 1994) sampled with a rate of 0.2 Hz from the relative barometer and the STS-1/Z were used for this analysis, because these data were known from a previous analysis to contain little seismic activity. The seismogram was detided by a least squares fit to a few sinusoids with the frequencies of the major tides. All earthquake signals were left in the seismometer data during this analysis. The time series were chopped into 8192-sample windows, hanned and Fourier transformed. The windows overlapped by 7/8 of their length. The auto- and cross-powerspectral densities were computed and averaged over all these windows resulting in estimates of the transfer-function as a function of frequency as well as of coherency. The transfer-function was instrumentally corrected to represent the admittance from barometric pressure to vertical

acceleration and was further smoothed by boxcar averaging over 9 adjacent estimates. The result with a clear minimum between 2.5 and 4 mHz is shown in Fig. 8. At frequencies above the minimum the admittance rises proportional to frequency squared as predicted by the IBPM. At frequencies below the minimum it approaches the constant value of eq. (1). The insert in the figure shows the coherency as a function of frequency. Also shown in the figure are four models for the admittance: the simple Bouguer model BPM (eq. (2)), the Bouguer model including the inertial effect IBPM (eq. (4)) using D = 13.5 km and $\mu = \lambda$ = 50 GPa, the modified Warburton-Goodkind model WG77 (eq. (9)) using a homogeneous atmosphere with scale height H = 10 km and the elasticity enhanced by 30 %, and finally the acoustic-gravity wave model AGW (eqns. (13), (15) and (16)) with $\mu = \lambda$ = 100 GPa and a horizontal phase velocity c_h = 80 m/s. These parameters were chosen by trial and error in order to roughly bring the notches to the vicinity of the minimum in the experimental admittance. The coherency does not attain values close to one at any frequency and above the minimum the two variables are essentially incoherent. Only a fraction of the total noise - a small one at the higher frequencies - is thus related to the local atmospheric pressure.

A second example obtained in the same way as for Fig. 8 is shown in Fig. 9. The time series in this case are from February 1, 0:00:00.0 GMT to March 27, 23:59:55.0 GMT in 2005. During this time period the breathing mode ${}_0S_0$ of the earth excited by the disastrous N-Sumatra - Andaman Islands earthquake was still clearly visible by eye on the vertical seismograms and this causes the zero coherency at 0.8146 mHz. The parameters for the models in the case here are: D = 22.5 km and μ = 50 GPa for the IBPM; H = 10 km and the elasticity of the model multiplied by 2.5 for WG77, μ = 60 GPa and c_h = 25 m/s for the AGW, again those were adjusted by trial and error to get the minimum close to the dip in the observed curve.

The two different IBPMs overpredict the experimental admittances for both cases at frequencies below and above the minimum. Experimental admittances for high quality gravimeters in essentially all cases were found to be below the constant in eq. (1). At BFO a small reduction is expected because the seismic sensors are 170 m below the surface, so the changing atmosphere is further away. If for the IBPM the ratio of crustal rigidity to thickness is lowered to bring the model admittance closer to the experimental one at low frequencies, the minimum will move towards lower frequencies and consequently the high frequency admittance will increase. It is not possible to adjust the model at all frequencies to the observed admittances. It was discussed in section 4.1 that the high frequency prediction by this model will be too high, because the horizontal scale of atmospheric disturbances is not considered in the model.

The WG77 used for Fig. 8 performs fairly well below the minimum but underpredicts the observed high frequency admittance greatly. The displacements due to the loading had to be increased by 30 % with respect to the original model to get the minimum about right. The variant used in Fig. 9 fits the observed admittance almost perfectly. However, the displacements here had to be multiplied by a factor of 2.5 to achieve this. The AGWs in both cases provide the position of the minimum but underpredict the admittances above and below it.

From the lack of coherency at frequencies higher than the minima in both cases it is obvious that here noise sources other than the local barometric pressure are dominating. From the work by Ekström (2001) and Nishida et al. (2002) it is clear that

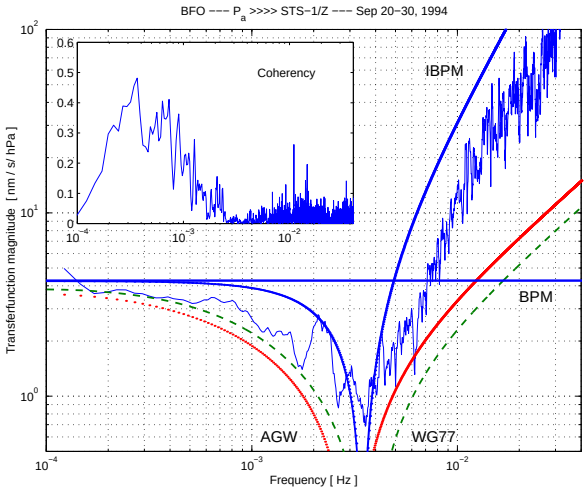

Fig. 8. Experimental admittance between local atmospheric pressure and vertical acceleration vs. frequency for data from September 20, 0:00:00.0 UTC to September 30, 23:59:55.0 UTC, 1994 (solid noisy curve). Model admittances for BPM, IBPM, WG77 and AGW, parameters were adjusted by trial and error in order to bring the minimum close to the observed one. See discussion in text. Insert shows coherency vs. frequency for experimental time series.

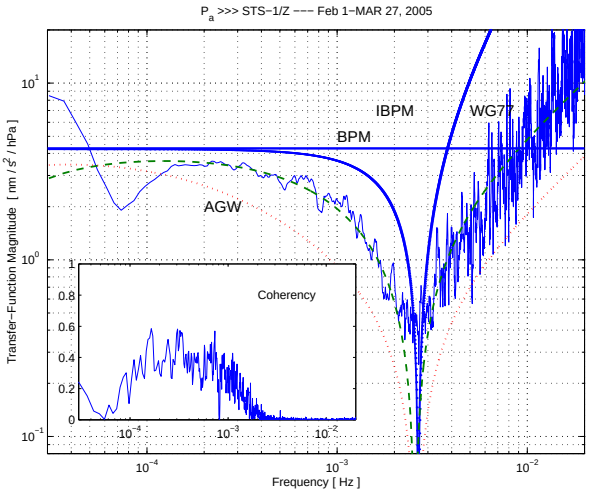

Fig. 9. Experimental admittance between local atmospheric pressure and vertical acceleration vs. frequency for data from February 1, 0:00:00.0 UTC to March 27, 23:59:55.0 UTC, 2005 (solid noisy curve). Model admittances for BPM, IBPM, WG77 and AGW, parameters were adjusted by trial and error in order to bring the minimum close to the observed one. See discussion in text. Insert shows coherency vs. frequency for experimental time series.

propagating Rayleigh waves provide a most important contribution.

On November 2, 2004 an interesting observation was made at BFO. Fig. 10 shows records from 3 broadband seismometers, a gravimeter and 3 strainmeters as well as from a relative barometer. The barometer shows a nice wavetrain between 13:30 and 14:00 GMT which can also clearly be seen in the horizontal seismometer and strainmeter traces. However, the two vertical accelerometers almost simultaneously show a clearly dispersive wavetrain with essentially twice the frequency of the waves in pressure. The pressure signal should also be seen in the vertical

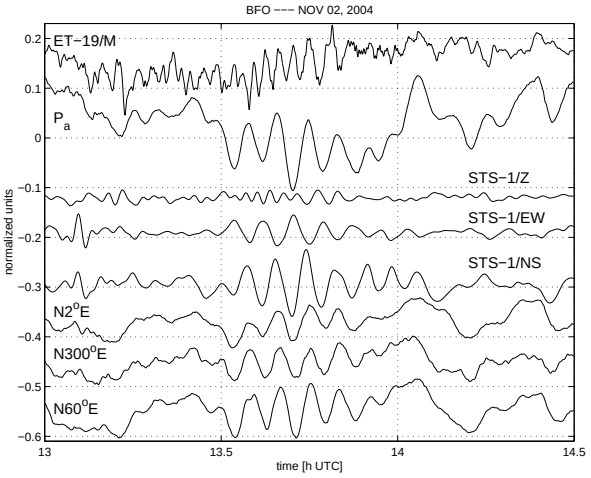

Fig. 10. Records from BFO between 13:00 and 14:30 GMT on November 2, 2004. From top to bottom these are, with peak-to-peak amplitudes at around 13:45: LCR-gravimeter ET-19 (mode-filter, 2.7 nm/s^2), relative barometer (0.30 *hPa*), STS-1/Z (2.0 nm/s^2), STS-1/EW (7.5 nm/s^2), STS-1/NS (15 nm/s^2)and 3 10-m invarwire-strainmeters ($N2^oE$: $0.13 \cdot 10^{-9}$, $N300^oE$: $0.15 \cdot 10^{-9}$, $N60^oE$: $0.22 \cdot 10^{-9}$). The STS-1 data were lowpass filtered with a cutoff frequency of 10 *mHz* before plotting. Note the frequency difference in the wavetrains in pressure, horizontal seismometers and strainmeters on one hand and the two vertical accelerometers on the other hand. For the seismometers the signal amplitude is given in acceleration, since this is not ambiguous at the frequencies of the wavetrains (Table 1).

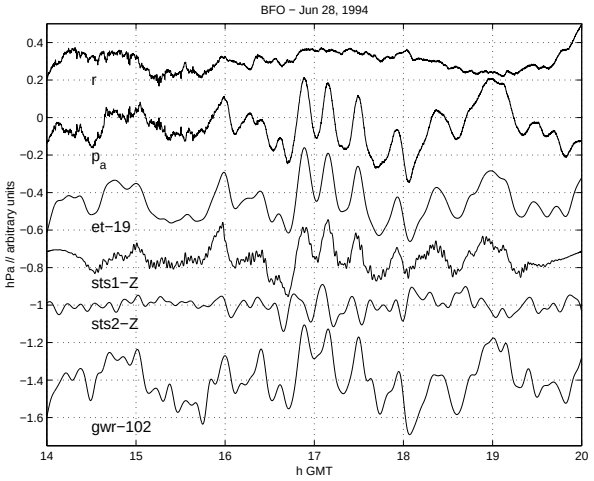

Fig. 11. Records from BFO on June 28, 1994, 14:00 to 20:00 GMT showing an atmospheric pressure oscillation and its effects on vertical accelerometers. Traces are from top to bottom: residual gravity (r, LCR ET-19 with 3.5 $nm/s^2 \cdot P_a$ subtracted), local atmospheric pressure (P_a, hPa), LaCoste-Romberg gravimeter (et-19), STS-1/Z, STS-2/Z, superconducting gravimeter (gwr-102). Very long periods (tides) were removed from all traces using polynomials (up to order 5). A butterworth low-pass filter with cutoff-frequency of 2.5 mHz was applied to sts-2/Z and gwr-102. The peak-to-peak amplitude of the oscillation at 17:00 are estimated to 0.29 hPa and 1.1 nm/s^2 and the frequency corresponds to 0.93 mHz. Note the efficiency of the pressure correction. No instrumental corrections were applied to the STS-2/Z data, while the STS-1/Z data were instrumentally corrected to represent acceleration.

record as in the examples below, but it is either missing completely or anyhow so small that it cannot be identified. On close inspection the wavetrain in the vertical component turns out to be the R_3 Rayleigh wave from the earthquake under Vancouver Island, Canada (M_w 6.6, 10:02:16 GMT) which is prominent in the vertical records, while it is masked by the atmospheric oscillation in the horizontals. The spectrum of the pressure waves is concentrated near 3.2 mHz with a power halfwidth of 1.3 mHz, while the power in the R_3 wave is spread between 3.9 and 7.8 mHz. This "missing" wave in the vertical records can be explained by the notch in the admittance for those components.

Another example is presented in Fig. 11. In 1994 four different vertical accelerometers were operating at BFO (Richter et al. 1995). Records of those are compared with the local barometric pressure for the dispersive wavetrain probably representing an AGW. The largest quasi-harmonic oscillations have frequencies below 1 mHz and are especially clear in the record from LaCoste-Romberg gravimeter ET-19. The top trace presents the difference between ET-19 vertical acceleration and barometric pressure times 3.5 $nm/s^2/hPa$.

The reduction of noise by the application of the simple Bouguer plate model is impressive in this case. This signal was already discussed by Neumann (1997) and Neumann and Zürn (1999), also for horizontal components and strains. Richter et al. (1995) compared the SNRs of the four instruments for the slowest free oscillations of the earth after the deep N-Bolivia quake (June 9, 1994, M_w 8.2) and found the superconducting gravimeter and the STS-2/Z inferior to the other two at these periods. This is reproduced in the traces in Fig. 11. While the amplitudes of the pressure oscillations in Figs. 10 and 11 are similar, the observed vertical acceleration amplitudes are quite different. The frequencies here are clearly in the regime where the Newtonian attraction dominates the other effects.

Another example of pressure oscillations is shown in Fig. 12. The dominant frequency in this case is at 3.0 mHz with a halfwidth of about 1.0 mHz. The bottom trace was obtained by subtracting the pressure from gravity with a factor of 1.5 $nm/s^2/hPa$. This is significantly lower than the factor in the case above. It is also evident, that with this factor only the 3 mHz - energy is reduced in the record, while the longer periods present in the gravity would need larger factors. Speculatively, this is probably caused by the proximity of the frequency content of the wave to the notch in the response of the vertical accelerometers.

The pressure pulse shown in Fig. 13 together with the effects on the vertical accelerometers at BFO has a broad spectrum in contrast to the examples above. BFO operates a rain gauge which integrates rainfall over intervals of 4 minutes. The pressure pulse was accompanied by a temperature drop of 4 to 5 degrees centigrade and rainfall of 2 and 1.5 mm in the first and second interval of the pulse. Light thunder was observed. Many thunderstorms have been observed at BFO during 30 years, but none other showed such a beautiful pulse shape in pressure.

The examples above suffer from the fact, that only local pressure is available to study them. A sensitive small microbarograph array with a typical dimension of only very few *kms* (Egger et al. 1993, Nishida et al. 2005) would be very helpful to improve the understanding of these noise sources in terms of propagation direction and horizontal speeds. Such an array is in the preparation stage at BFO.

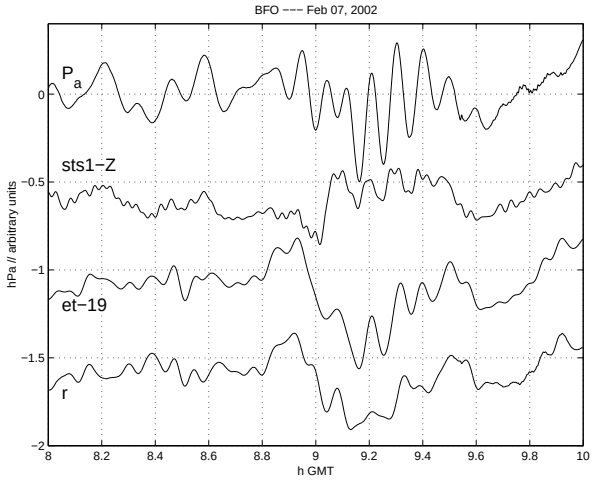

Fig. 12. Records from BFO on February 7, 2002, 8:00 to 10:00 GMT showing an atmospheric pressure oscillation and its effects on two vertical accelerometers.Traces are from top to bottom: barometric pressure in hPa (detrended), STS-1/Z (corrected for instrumental response to represent acceleration) and ET-19 (detrended) without and with pressure correction. All accelerometer time series were low-pass filtered at 5 mHz. The pressure correction factor used for ET-19 was here 1.5 $nm/s^2/hPa \cdot P_a$, in contrast to the one used for the data in Fig. 11. The wavetrain between 9:00 and 9:36 GMT has a dominant frequency of 3.0 mHz and a spectral halfwidth of about 1 mHz. The peak-to-peak amplitudes of the oscillation at 9.2 h GMT are 0.55 hPa for P_a, 0.88 nm/s^2 for STS1-Z and 1.03 nm/s^2 for ET-19, respectively.

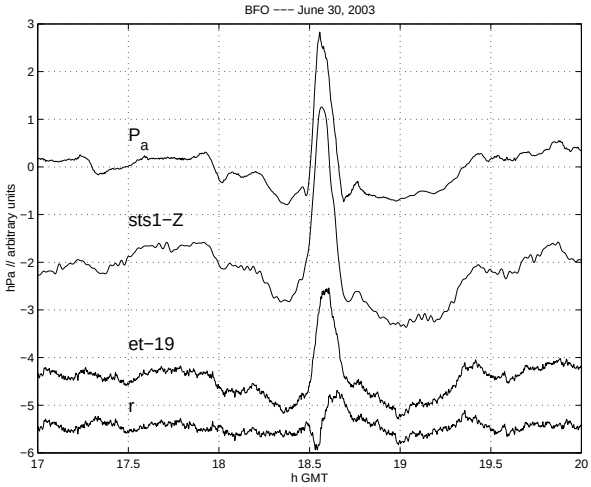

Fig. 13. Impulsive pressure event recorded at BFO at 18:30 GMT on June 30, 2003. Traces from top to bottom are: barometric pressure in *hPa*, STS1-Z (corrected for instrumental response to represent acceleration), ET-19 (detrended) without and with subtracting 2.65 $nm/s^2/hPa \cdot P_a$. The pressure pulse is not gone completely from the gravity record. The pressure pulse has an amplitude of about 3 *hPa* and lasts $\approx$ 12 *minutes*. The pulse amplitude in acceleration is about 10 nm/s^2.

6 DISCUSSION

Realizing that the above models of atmospheric phenomena are rather simple, we maintain that the physical effects discussed are very realistic no matter what goes on in the atmosphere. At long periods vertical accelerometers at very good stations must sense these effects, which they cannot be shielded from by any means. The cancellation also must take place and is very likely to cause the minimum in acceleration noise near 3 mHz at the best stations. However, the exact notch-frequency will be variable spatially and temporally. Variation in time occurs because atmospheric behaviour is highly variable and different phenomena are active at different times (from stable high pressure cells to frontal passages to thunderstorms, tornados and hurricanes). The occurrence of such phenomena shows different statistics in different climate zones. Additional effects exist as demonstrated for instance by the observations by Meurers (2000) and Simon (2003). Since the reaction of the site depends on the elastic structure of the crust, each station would have its own notch-frequency even if the atmospheric phenomenon above it would be identical.

This variability of the notch-frequency would be interesting to study but clearly the notch is covered with noise and/or signals of different origin as discussed in the introduction and in Zürn and Widmer-Schnidrig (2003) and therefore this is impossible.

The Rayleigh waves from Mount Pinatubo had frequencies of 3.7 and 4.4 mHz (Kanamori and Mori 1992, Widmer and Zürn 1992). The first of these authors estimated that a peak-to-peak pressure oscillation of 3 hPa on a circular area with 38 km radius could explain the signals. These frequencies are very close to the notch in the admittance and were observed worldwide. No local accelerometer records exist to the best of our knowledge, unfortunately, and it would have been very interesting to see such records. The paradoxical situation could have occurred that no signal would be observed locally, but at teleseismic distances clear oscillations are detected and the local accelerometers would only have seen those oscillations after the waves circled the globe at least once, three hours later. However, the physics of the source and the structure of the density variations is largely unknown and therefore this paradox is highly speculative (see Kanamori et al. 1994 and Lognonné et al. 1998 for a discussion of the source).

Acknowledgements Thanks go to Herbert Wilmes and Peter Wolf, Bundesamt für Kartographie und Geodäsie, Frankfurt for providing the records from their superconducting gravimeters. We thank Ruedi Widmer-Schnidrig, Udo Neumann, Corinna Kroner, Thomas Jahr and especially Thomas Forbriger and Holger Steffen for discussions. Financial support by the "Deutsche Forschungsgemeinschaft" under grants number KR 1906/3-1 and WE 2628/1-1 is gratefully acknowledged.

References

Agnew, D. C. (1986). Strainmeters and Tiltmeters. *Rev. Geophys.*, **24:** 579 - 624.

Agnew, D. C., Berger, J. (1978). Vertical Seismic Noise at Very Low Frequencies. *J. geophys. Res.*, **83:** 5420 - 5424.

Banka, D., Crossley, D. (1999). Noise Levels of Superconducting Gravimeters at Seismic Frequencies. *Geophys. J. Int.*, **139:** 87 - 97.

Beauduin, R., P. Lognonné, J. P. Montagner, S. Cacho, J. F. Karczewski and M. Morand (1996). The Effects of Atmospheric Pressure Changes on Seismic Signals or How to Improve the Quality of a Station. *Bull. seism. Soc. Am.*, **86**: 1760 - 1769.

Berger, J., P. Davis and G. Ekström (2004). Ambient Earth Noise: A Survey of the Global Seismographic Network. *J. geophys. Res.*,**109**, B11307, doi: 10.1029/2004JB003408.

Boy, J.-P., Hinderer, J., Gegout, P. (1998). Global atmospheric loading and gravity. *Phys. Earth planet. Inter.*, **109:** 161 - 177.

Dahlen, F. A., Tromp, J. (1998). *Theoretical Global Seismology*. Princeton University Press, Princeton, New Jersey, 1025 pp.

Dobrin, M. B. (1960). *Introduction to Geophysical Prospecting*. 2nd edition, McGraw-Hill Book Company, New York, 446 pp.

Egger, J., Wamser, C., Kottmeier, C. (1993). Internal atmospheric gravity waves near the coast of Antarctica. *Boundary-Layer Meteorology*, **66**: 1 - 17.

Ekström, G. (2001). Time domain analysis of Earth's long-period background seismic radiation. *J. geophys. Res.*, **106**: 26,483 - 26493.

Fortak, H. (1971). *Meteorologie*. Carl Hebel Verlagsbuchhandlung, Berlin und Darmstadt.

Freybourger, M., Hinderer, J., Trampert, J. (1997). Comparative study of superconducting gravimeters and broadband seismometers STS-1/Z in seismic and subseismic frequency bands. *Phys. Earth planet. Inter.*, **101:** 203 - 217.

Fukao, Y., Nishida, K., Suda, N., Nawa, K., Kobayashi, N. (2002). A theory of the Earth's background free oscillations. *J. geophys. Res.*, **107(B9)**, 2206, doi: 10.1029/2001JB000153.

Gilbert, F., 1980. An introduction to low-frequency seismology. In Dziewonski, A. M. and Boschi, E. (eds.), *Fisica dell'interno della Terra, Rendiconti della Scuola Internazionale di Fisica "Enrico Fermi"*, Varenna, Italy, course LXXVII, p. 41 -81, North-Holland, Amsterdam.

Gossard, E. E., Hooke, W. H. (1975). *Waves in the Atmosphere*. Elsevier, Amsterdam, 456 pp.

Kanamori, H., Mori, J. (1992). Harmonic excitation of mantle Rayleigh waves by the 1991 eruption of Mt. Pinatubo, Philippines. *Geophys. Res. Lett.*, **19:** 721 - 724.

Kanamori, H., Mori, J., Harkrider, D. G. (1994). Excitation of Atmospheric Oscillations by Volcanic Eruptions. *J. geophys. Res.*, **99:** 21947 - 21961.

King, G. C. P, Zürn, W., Evans, R., Emter, D. (1976). Site Corrections for Long-Period Seismometers, Tilt- and Strainmeters. *Geophys. J. R. astr. Soc.*, **44:** 405 - 411.

Lognonné P., Clévédé, E., Kanamori, H. (1998). Computation of seismograms and atmospheric oscillations by normal-mode summation for a spherical earth model with realistic atmosphere. *Geophys. J. Int.*, **135:** 388 - 406.

Meurers, B. (2000). Gravitational effects of atmospheric processes in SG gravity data. *Cah. Centre Europ. Geodyn. Seismol.*, **17:** 57 - 65.

Müller, T. (1981). Die Untersuchung von langperiodischen Schweresignalen beim Durchzug von Wetterfronten. Diploma thesis, Karlsruhe University.

Müller, T. and W. Zürn (1983). Observation of gravity changes during the passage of cold fronts. *J. Geophys.*, **53**: 155 - 162.

Nappo, C. J. (2002). An Introduction to Atmospheric Gravity Waves. *Int. Geophys. Ser.*, **85**, Academic Press, Amsterdam, 276 p.

Nawa, K., Suda, N., Fukao, Y., Sato, T., Aoyama, Y., Shibuya, K. (1998). Incessant excitation of the Earth's free oscillations. *Earth Planets Space*, **50**: 3 - 8.

Neumann, U. (1997). Langperiodisches seismisches Rauschen durch atmosphärische Wellen. Diploma thesis, Geophysics, University of Karlsruhe, 137 p.

Neumann, U., Zürn, W. (1999). Gravity signals from atmospheric waves and their modeling. *Bull. Inf. Marées Terrestres*, **131**: 10139 - 10152.

Nishida, K., Fukao, Y., Watada, S., Kobayashi, N., Tahira, M., Suda, N., Nawa, K., Oi, T., Kitajima, T. (2005). Array observation of background atmospheric waves in the seismic band from 1 mHz to 0.5 Hz. *Geophys. J. Int.*, **162**: 824 - 840. doi: 10.1111/j.1365-246X.2005.02677.x

Nishida, K., Kobayashi, N., Fukao, Y. (2000). Resonant Oscillations Between the Solid Earth and the Atmosphere. *Science*, **287:** 2244 - 2246.

Nishida, K., Kobayashi, N., Fukao, Y. (2002). Origin of Earth's ground noise from 2 to 20 mHz. *Geophys. Res. Lett.*, **29**, doi: 10.1029/2001GL013862.

Peterson, J. (1993). Observations and Modeling of Seismic Background Noise. *U. S. Geol. Surv., Open-File Rep.*, **93-322:** 1 - 45.

Rabbel, W., Zschau, J. (1985). Deformations and Gravity Changes at the Earth's Surface Due to Atmospheric Loading. *J. Geophysics*, **56**: 81 - 99.

Rhie, J. and B. Romanowicz (2004). Excitation of earth's incessant free oscillations by Atmosphere-Ocean-Seafloor coupling. *Nature*, **431:** 552 - 556.

Richter, B., H.-G. Wenzel, W. Zürn and F. Klopping (1995). From Chandler wobble to free oscillations: comparison of cryogenic gravimeters and other instruments in a wide period range. *Phys. Earth planet. Inter.*, **91:**, 131 - 148.

Simon, D. (2003). Modelling of the gravimetric effects induced by vertical air mass shifts. *Mittlg. Bundesamt Kartogr. Geod.*, **21:** 1 - 132.

Sorrells, G. G. (1971). A preliminary investigation into the relationship between long-period seismic noise and local fluctuations in the atmospheric pressure field. *Geophys. J. R. astr. Soc.*, **26**: 71 - 82.

Suda, N., Nawa, K., Fukao, Y. (1998). Earth's Background Free Oscillations. *Science*, **279:** 2069 - 2091.

Tanimoto, T. (1999). Excitation of Normal Modes by Atmospheric Turbulence: Source of Long Period Seismic Noise. *Geophys. J. Int.*, **136:** 395 - 402.

Tanimoto, T. (2005). The Oceanic Excitation Hypothesis for the Continuous Oscillations of the Earth. *Geophys. J. Int.*, **160**: 276 - 288.

Tanimoto, T., Um, J. (1999). Cause of continuous oscillations of the Earth. *J. geophys. Res.*, **104:** 28723 - 28739.

Tanimoto, T., Um, J., Nishida, K., Kobayashi, N. (1998). Earth's continuous oscillations observed on seismically quiet days. *Geophys. Res. Lett.*, **25:** 1553 - 1556.

Van Camp, M. (1999). Measuring seismic normal modes with the GWR C021 superconducting gravimeter. *Phys. Earth planet. Inter.*, **116:** 81 - 92.

Virtanen, H. (1996). Observations of free oscillations of the Earth by superconducting gravimeter GWR T020. *Acta Geod. et Geophys. Hung.*, **31**: 423 - 431.

Warburton, R. J., Goodkind, J. M. (1977). The influence of barometric pressure variations on gravity. *Geophys. J. R. astr. Soc.*, **48**: 281 - 292.

Widmer-Schnidrig, R. (2003). What Can Superconducting Gravimeters Contribute to Normal-Mode Seismology. *Bull. seism. Soc. Am.*, **93:** 1370 - 1380.

Widmer, R., Zürn, W. (1992). Bichromatic excitation of long-period Rayleigh and air waves by the Mount Pinatubo and El Chichon volcanic eruptions. *Geophys. Res. Lett.*, **19:** 765 - 768.

Wielandt, E., Streckeisen, G. (1982). The Leaf-Spring Seis-

mometer: Design and Performance. *Bull. Seism. Soc. Am.*, **72A:** 2349 - 2368.

Zürn, W. (2002). Simplistic models of vertical seismic noise above 0.1 mHz derived from local barometric pressure. *Bull. Inf. Marées Terrestres*, **137**: 10867 - 10874.

Zürn, W., Laske, G., Widmer-Schnidrig, R., Gilbert, F. (2000). Observation of Coriolis coupled modes below 1 mHz. *Geophys. J. Int.*, **143**: 113 - 118.

Zürn, W. and R. Widmer (1995). On noise reduction in vertical seismic records below 2 mHz using local barometric pressure. *Geophys. Res. Lett.*, **22**: 3537 - 3540.

Zürn, W., Widmer-Schnidrig, R. (2003). Vertical Acceleration Noise at Seismic Frequencies. *Cah. Centr Europ. Geodyn. Seismol.*, **22:** 123 - 127.